Special Issue
Martensitic and Bainitic Transformations in Steels; Fundamentals and Their Applications

ISIJ International, Vol. 64 (2024), No. 2, pp. 212–217
https://doi.org/10.2355/isijinternational.ISIJINT-2023-163

Determination of Microscopic Strain Distribution in the Martensitic Transformation of Fe-31Ni Alloy Plates Using the Micro-grid Marker Method

Tatsuya MORIKAWA,[1)*] Akinobu SHIBATA,[2)] Naoto NAKAMURA,[3)] Masaki TANAKA[1)] and Kenji HIGASHIDA[1)]

1) Department of Materials, Kyushu University, 744 Motooka, Nishi-ku, Fukuoka, 819-0395 Japan.
2) National Institute for Materials Science, 1-2-1 Sengen, Tsukuba, Ibaraki, 305-0047 Japan.
3) Graduate student, Kyushu University. Now at JFE Steel Corporation, 1 Kokan-cho, Fukuyama, Hiroshima, 721-8510 Japan.

(*Received April 28, 2023; Accepted September 7, 2023; Published January 30, 2024*)

The strain distribution due to martensitic transformation in a Fe–Ni alloy was investigated using high-precision markers drawn via electron-beam lithography. This study focused on the strain distribution within the lenticular martensite plate, which developed immediately below the martensite start temperature.

The strain in the central region of lenticular martensite was determined to be greater than that near the interface boundary by measuring the displacement at each intersection of the grid markers. This finding is consistent with the shape strain distribution predicted by the phenomenological theory of martensitic transformation based on the microstructure observations.

KEY WORDS: martensitic phase transformation; plastic deformation; electron backscattering diffraction (EBSD); electron beam lithography.

1. Introduction

Material strengthening based on the martensitic transformation of austenite is an effective method of improving the mechanical properties of steel.[1–4] This is achieved by refining crystal grains and the strengthening lattices with solid solute carbon, while introducing excessive dislocations.

The phenomenological theory of martensite crystallography (PTMC) can explain the orientation of the crystallographic habit plane after transformation, the direction and amount of shape strain, and the relationship between the martensite and austenite crystallographic orientations.[5,6] PTMC, which considers two types of slip in lattice-invariant deformation, is applied to predict the crystallographic features of lath martensite, However, many combinations of lattice-invariant deformations result in the {252}-type habit plane with crystal plane orientations close to that of lath martensite.[7–9]

The orientation of the habit plane in thin-plate martensite is adequately explained by the early Wechsler-Lieberman-Reed method or the Bowles-Mackenzie methods,[5,6] that is PTMC with single lattice-invariant deformation. However, lenticular martensite exhibits complicated microstructures that include a twinned dense structure called a midrib in the central part of the plate, a twinned region outside of the midrib, and an untwinned region near the interface boundary.[10,11] The habit plane of lenticular martensite corresponds to a midrib plane, and PTMC can explain its orientation with single lattice-invariant deformation. In addition, several sets of dislocations were observed in the untwinned regions, PTMC can explain the orientation of faceted interfaces observed in lenticular martensite with a relatively high martensite start (Ms) tempertature, which can be explained by considering PTMC with lattice-invariant deformation caused by two types of experimentally identified slip systems. To experimentally verify the validity of the various martensitic transformation models, such as PTMC, it is essential to establish a method for quantitatively measuring the shape strain tensor. Nevertheless, only a few studies have attempted to measure this shape strain experimentally,[12,13] even though the direction and degree of shape strain can be predicted using PTMC.

On the other hand, several recent studies have examined the influence of a material's local plastic deformation state on its macroscopic mechanical properties. Digital Image Correlation (DIC) method has recently been attracting attention as a method for capturing local strain. The DIC is a method to trace the surface aspect of a material under

* Corresponding author: E-mail: morikawa.tatsuya.771@m.kyushu-u.ac.jp

plastic deformation and quantify the amount of deformation. By obtaining the surface strain distribution, knowledge of the effect of dispersed precipitates on the transformation behavior,[14] the effect of crystal orientation on strain accumulation,[15] and the effect of strain distribution on fatigue crack propagation has been obtained.[16,17] Furthermore, the quantification of the deformation of slip bands has been achieved.[18] In particular, for dual-phase steel, the effects of the strain concentration in each phase on the mechanical properties have been investigated by measuring the local strain distributions of the hard and soft phases.[19,20] We also examined the relationship between the local strain distribution and the mechanical properties using a method whereby specific grid markers (on the order of nanometers) were drawn onto the smoothed surface of a material. Electron-beam lithography was used to draw these markers, and their displacement upon plastic deformation was measured to determine the local strain distribution.

In the present study, we have used this precise marker method to determine the plastic strain distribution associated with the thermally induced martensitic transformation in Fe-31mass%Ni alloy, representing a lenticular martensite with a width of 5–20 μm. We report the characteristics of the measured strain distribution induced by martensitic transformation, which was experimentally determined using a precise marker method. Furthermore, based on observations of microstructures, such as deformation twins and dislocations resulting from lattice-invariant deformation, we demonstrate the validity of the estimated shape strain derived from the PTMC.

2. Experimental Procedure

We employed a Fe-31mass%Ni alloy (C < 0.002) in the present study. The alloy was homogenized at 1 473 K for 86.4 ks in a vacuum and then cold-rolled into a sheet of 0.5 mm in thickness. The sheet was then austenitized at 1 473 K for 3.6 ks in a vacuum, and then water-quenched. A specimen measuring 12 mm × 12 × 0.5 mm^3 was cut from the sheet by spark cutting. To examine the local strain distribution in the alloys due to martensitic transformation, we employed high-precision grid gold markers with a width of 70 nm, using electron-beam lithography (EBL).[21]

For electron beam lithography, the sample surface was subjected to ordinary mechanical polishing followed by polishing with colloidal silica. The EBL process is schematically shown in **Figs. 1**(a)–1(e). First, the resist was spin-coated onto an electro-polished surface (Fig. 1(a)). Second, a pattern was drawn on the resist by using an electron beam (Fig. 1(b)), and the resist exposed to the electron beam was removed using a developer (Fig. 1(c)). Au was then evaporated onto the surface (Fig. 1(d)), after which the remaining resist was dissolved (Fig. 1(e)). The patterns obtained using these markers are shown in Fig. 1(f). Figure 1(g) shows an SEM image of the pattern, where the side of the square was 500 nm in length.

The specimen was cooled to 218 K, slightly below the Ms temperature (223 K),[22] to obtain a microstructure with partially formed lenticular martensite. The shapes of the markers were observed using field-emission scanning electron microscopy (FESEM) secondary electron images, and

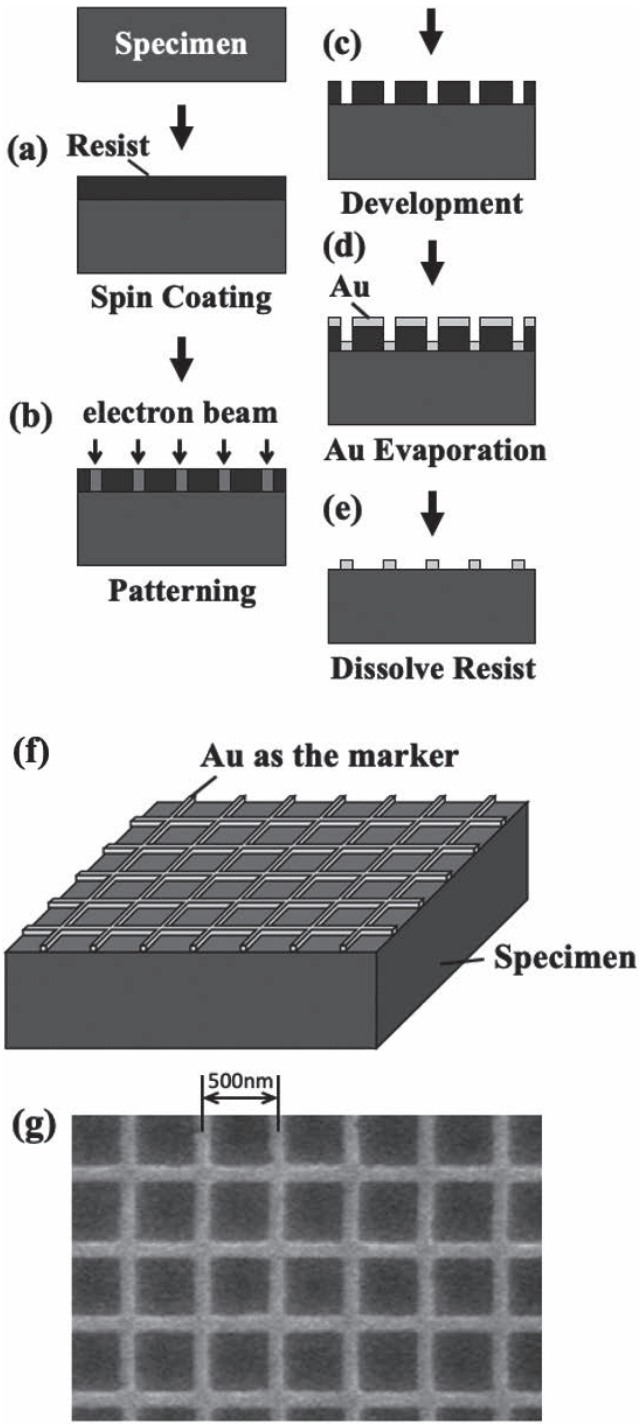

Fig. 1. (a)–(e) Schematic illustrations showing the process whereby precise grid markers are drawn by using electron beam lithography. (f) Perspective of the markers on the specimen surface. (g) SEM image of markers and dimensions of the pattern.

the orientation distribution and configuration of the phase were detected using scanning electron microscopy-electron backscattering diffraction (SEM-EBSD). The displacements of the squares' vertices in the pattern were measured. The Green-Lagrange shear strain was evaluated based on the displacements of the vertices of each square.

3. Results

Figures 2(a) and 2(b) show the orientation maps obtained

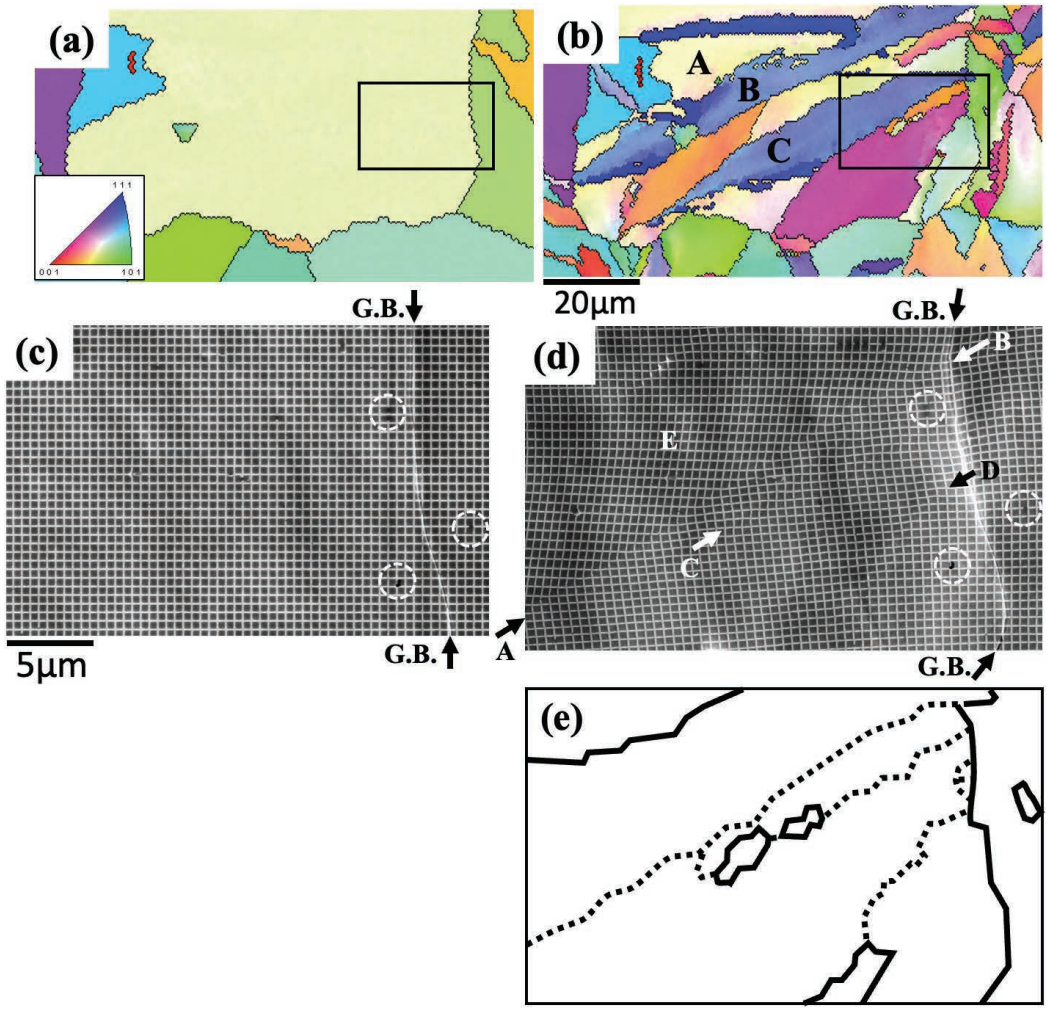

Fig. 2. (a), (b) Orientation maps obtained by SEM-EBSD for a given area of the specimen before transformation and after quenching at 218 K, respectively. (c), (d) SEM images of the areas corresponding to the black squares in Figs. 2(a) and 2(b), respectively. (e) A schematic illustration of the martensite configuration corresponding to Fig. 2(d).

by SEM-EBSD for the same area of the specimen before and after sub-zero cooling to 218 K, respectively. The colors in the figure indicate the orientation relative to the direction normal to the specimen surface, with each color corresponding to the crystal orientation shown as a stereo triangle in the lower left of the figure. The black lines in Fig. 2(a) indicate the austenite grain boundaries in the specimen before transformation, when no martensite was observed. In contrast, in Fig. 2(b), elongated grains with a new orientation are formed in many of the austenite grains in the figure, indicating a partial martensitic transformation. After sub-zero cooling to 218 K, the area fraction of martensite was approximately 25%. Several martensite plates with different orientation are formed. The color of part of the martensite and that the austenite near the martensite gradually changed. This suggests that the plastic deformation within the martensite is not uniform and that part of the austenite also deforms with the transformation of the neighboring region.

On the other hand, Figs. 2(c) and 2(d) show SEM images of the areas corresponding to the black squares in Figs. 2(a) and 2(b), respectively. The arrows marked as G.B. on the right side of the figure indicate the position of the austenite grain boundary. Figure 2(e) shows the configuration of the martensite sites corresponding to Fig. 2(d), where the solid and broken lines indicate the interfaces between martensite and austenite, and the boundaries of the martensite plates, respectively. Before the transformation shown in Fig. 2(c), the markers drawn by electron-beam lithography were arranged in an orderly layout. However, some irregularities can be observed in this figure (indicated by white broken circles). The black arrows in the figure indicate the top and bottom ends of the austenite grain boundary. Figure 2(d) shows the marker's appearance in the area, including the region shown in Fig. 2(c), after the partial transformation to martensite. In Fig. 2(d), the marker irregularities are indicated by the broken circles, which are the same as those shown in Fig. 2(c). This suggests that the area shown in Fig. 2(d) includes that shown in Fig. 2(c) before the transformation. In Fig. 2(d), the marker lines bent abruptly at the positions indicated by arrows A and B, with the bending occurring across the figure from arrows A to B. In addition, the grid marker shears the area around the abrupt bend, and the direction of the shear in the region above the bend is opposite to that below the bend. The position at which the abrupt bend in the marker corresponds to the boundary between the martensite plates in the middle of Fig. 2(e) indicates that the shear directions in the plates differ. The bending of the marker line is also observed at the positions

indicated by arrows C and D in the figure corresponding to the martensite boundary observed in Fig. 2(b), which is similar to the region indicated by arrows A and B. As described above, it was possible to detect the difference in the manner of plastic deformation for each martensite plate owing to the martensitic transformation using the precise marker method described herein. Furthermore, a gentle curvature of the marker line was observed in the area indicated by E, suggesting that plastic deformation inside the martensite plate was non-homogeneous. This is consistent with the nonuniform orientation distribution inside each martensite plate, as shown in Fig. 2(b).

Figure 3(a) shows the distribution of the absolute value of the Green-Lagrange shear strain $|\varepsilon_{xy}|$ as calculated from the marker displacement in the xy orthogonal coordinate system shown in the figure. The area shown in Fig. 3(a) is nearly the same as that shown in Fig. 2(b), with regions A, B and C corresponding to those indicated in Fig. 2(b). Figure 3(b) shows the configuration of martensite corresponding to Fig. 3(a), where the solid and broken lines indicate the interfaces between martensite and austenite, and the boundaries between the martensite plates, respectively. As shown in Fig. 2, the plastic deformation associated with the martensitic transformation was detected using markers. When a relatively large deformation occurs, as in the case of a martensitic transformation, it is useful to estimate the Green-Lagrange shear strain. The colors in the figure indicate the strain magnitude, with the colors shown in the colored bar on the left side of the figure. In this strain distribution map, each square of the initial marker is colored to represent the strain value at that location, whereas the change in the shape of the marker is not reflected.

The area indicated by A in Fig. 3(a) corresponds to austenite, where the plastic strain barely increased. However, the strain increased considerably in the areas where martensitic transformation occurred, as shown in Fig. 3(a), particularly in the regions corresponding to the martensite plates indicated by B and C in Fig. 3(a). It should be noted that lenticular martensite plates B and C exhibit large strains in the middle of the plate, whereas the strain near the interface is relatively small. In particular, for the region corresponding to martensite plate B, the position in the middle of the plate, as indicated by the large arrow represents the value of the shear strain, which is approximately 0.2. Some squares in the middle of martensite plate C show strains above 0.15. Another region with large strain was also observed at the edge of the lenticular martensite (indicated by the small vertical arrows), where the martensite grew and reached to the grain boundary of the austenite. It is believed that when the edge of the martensite plate reaches the boundary, a considerable large plastic strain occurs to realize the continuity of the displacement at the grain boundary.

To clarify the strain distribution within the martensite plate, **Figs. 4**(a), 4(b) show the profiles of the shear strain between the two horizontal white arrows marked α and α', β and β' from that shown in Fig. 3(a), respectively. The horizontal axis indicates the distance whereas the vertical axis shows the absolute value of the shear strain in both figures, denoted by ε_{xy}. The strain in the middle of the martensite plate B increases to almost 0.2, while the strain values near the martensite/austenite interface appear to be 0.1 or less, as shown in Fig. 3(a). The strain in the middle of the martensite plate C was also more significant than that near the austenite-martensite interface, as shown in Fig. 3(a).

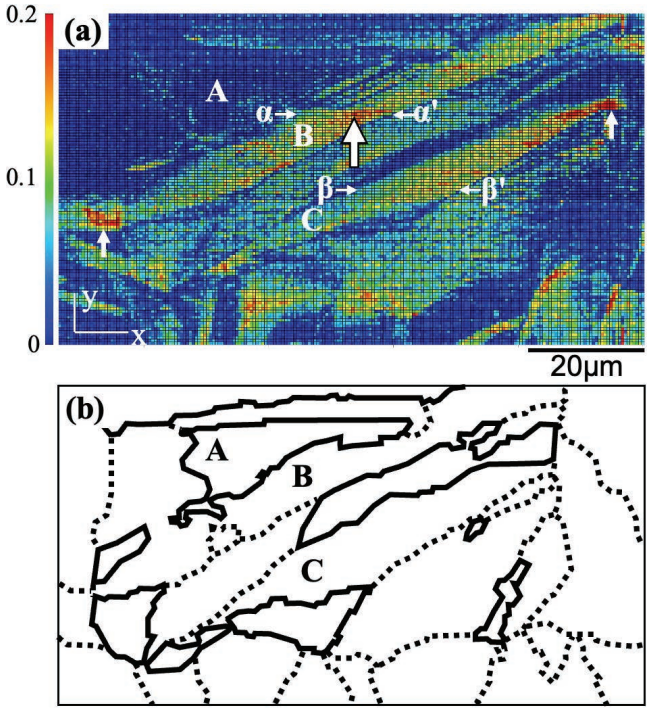

Fig. 3. (a) Plastic shear strain distribution map obtained for the specimen shown in Fig. 2. (b) A schematic illustration of the configuration of martensite corresponding to Fig. 3(a).

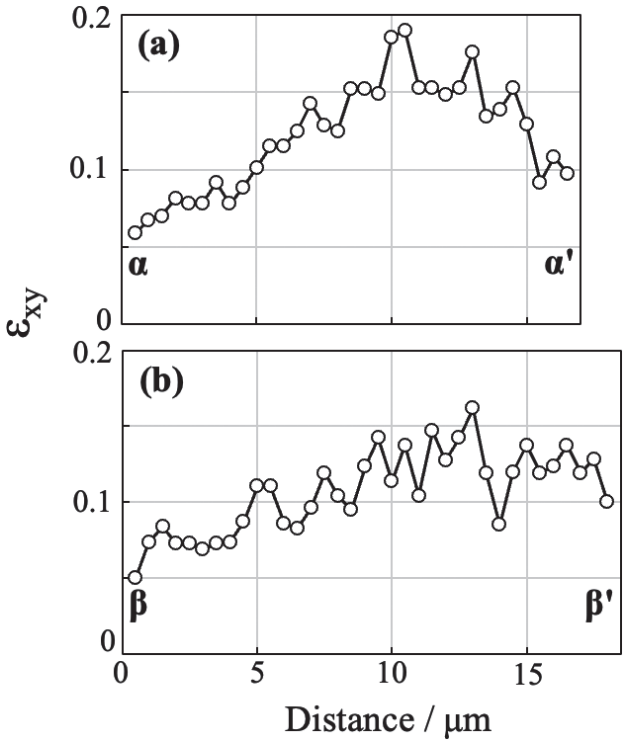

Fig. 4. Profiles of the shear strain between the two horizontal white arrows (a) α and α', (b) β and β', from those shown in Fig. 3(a).

4. Discussion

As mentioned above, in this study, we were able to quantify the strain inside each martensitic plate during the martensitic transformation induced by heat treatment of Fe–Ni alloys. The results show that there is a significant difference between the strain at the austenite-martensite interface and that inside the plate. This means that the electron-beam lithography-based fine-marker method used in this study was very useful in quantifying the strains associated with martensitic transformation. Because the shape strain estimated by the PTMC is shear strain, the experimentally observed surface displacement is considered to correspond to the shape strain if the shear direction is not perpendicular to the material surface. Therefore, in this chapter, we attempt to correlate the shape strain obtained by the PTMC with the observed surface shear strain.

The substructure of lenticular martensite in Fe-31Ni and Fe-33Ni alloys has been investigated in detail by Shibata *et al.* using transmission electron microscopy (TEM) and high-resolution electron microscopy (HREM) to clarify characteristics such as the slip plane and Burgers vectors of the dislocations on the martensite side on the martensite/austenite interface.[22] Two types of dislocations were found with different Burgers vectors on the interface between both phases; $\mathbf{b_1} = a/2[1\ \bar{1}\ \bar{1}]$ and $\mathbf{b_2} = a/2[11\ \bar{1}]$. Furthermore, when the slip deformation owing to the activation of these two types of dislocations was treated as a lattice-invariant deformation, the shape strain was calculated based on the PTMC as shown in **Fig. 5**. Although single slip was assumed to be a lattice-invariant deformation in the initial calculation method of shape strain,[5,6] two types of slip were identified in the observation; therefore, Fig. 5 shows the results based on a double shear model.[9–11]

Using PTMC, the plastic deformation associated with the transformation can be calculated using the shape strain tensor **F** as follows;

$$\mathbf{F} = \mathbf{RBP} \quad \text{..... (1)}$$

where **R** is a rigid body rotation matrix, **B** is a matrix representing the Bain deformation, and **P** is a matrix corresponding to the lattice-invariant deformation. When the lattice-invariant deformations are due to two types of slip, $\mathbf{P_1}$ and $\mathbf{P_2}$ are the matrices corresponding to the respective deformations, and Eq. (1) becomes

$$\mathbf{F} = \mathbf{RBP_1P_2} \quad \text{..... (2)}$$

The relationship between the shape strain obtained in this manner and the two types of lattice-invariant deformation is shown in Fig. 5.[23] The amounts of shear caused by the two types of lattice-invariant deformations $\mathbf{P_1}$ and $\mathbf{P_2}$ in Eq. (2) are expressed as s_1 and s_2, respectively. These correspond to activated slips with Burgers vectors $\mathbf{b_1}$ and $\mathbf{b_2}$ described above.

The horizontal axis in Fig. 5 denotes the amount of the slip s_1 owing to dislocation $\mathbf{b_1}$, whereas the vertical axis shows the amount of strain. The curves in this figure indicate the change in the calculated shape strain (solid line) and the strain s_2 (broken line) owing to dislocation $\mathbf{b_2}$ according to the change in s_1. Because the midrib (*i.e.* transformation twins) is formed in the middle of the lenticular martensite, the shear deformation is only due to s_1 ($s_2 = 0$). This is shown at the left end of the horizontal axis in Fig. 5, which corresponds to the midrib region; therefore, at $s_1 = 0.24$, $s_2 = 0$, the shape strain in the midrib region is estimated to be 0.23. In contrast, the minimum value of the shape deformation was 0.12, when $s_1 = 0.28$ and $s_2 = 0.11$. Because the value of $s_2 = 0.12$, according to the TEM observations near the interface between the martensite and austenite, is close to 0.11, it is considered that the shape strain near the interface decreases to approximately 0.12, which is the minimum value estimated by the PTMC. As mentioned above, by applying the TEM observation result of the dislocation in the vicinity of the interface between martensite and austenite to the PTMC, the distribution of the shape strain inside the lenticular martensite can be predicted to show that the shape strain is as significant as 0.23 at the midrib in the middle of the martensite plate, and as small as 0.12 in the vicinity of the interface.

The shear strain inside the lenticular martensite was measured using the precise marker method, and the resulting distribution is visualized in Fig. 3(a). The change of shear strain on the line along α-α' and β-β' that are shown in Fig. 3(a), are respectively profiled in Figs. 4(a) and 4(b), where the value of shear strain at the middle of the martensite plate is more significant than that near the interface. The shape strain during the martensitic transformation was calculated from the PTMC based on the shear plane, shear direction, and shear amount of the lattice-invariant deformation identified by TEM and RTEM observations at the martensite/austenite interface. The shape strain corresponding to the final plastic strain after the transformation strain was relaxed via lattice-invariant deformation. Therefore, within a single martensite plate, the shear strain on the observation plane estimated by capturing the marker displacement should correspond in magnitude to that on the observation plane. A comparison of Figs. 4 and 5 show good correspondence with the estimated shape strain inside the martensite plate.

As mentioned above, it is suggested that the fundamental process of the lattice-invariant deformation with the formation of lenticular martensite in the middle of the plate (where single shear due to twin deformation occurs) is different from that found in the vicinity of the interface, where double shear due to two types of slip deformation occurs.

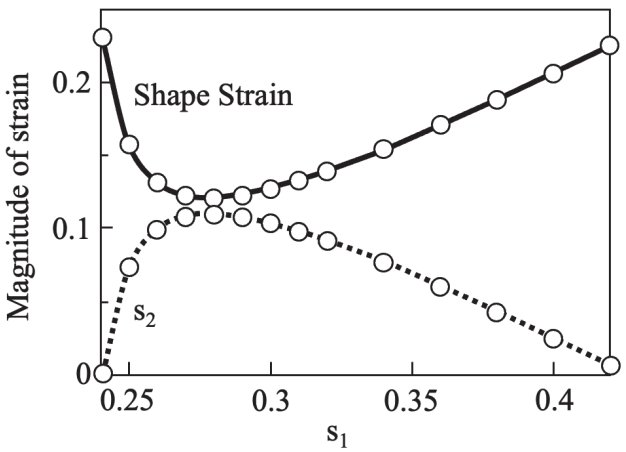

Fig. 5. Change in the magnitude of shape strain and s_2 with the magnitude of s_1.[17]

This is considered to be affected by an increase in the local temperature when the lenticular martensite grows further after the initial formation of the midrib.[24] When the shear direction of the shape strain was approximately parallel to the specimen surface, the strain obtained using the marker method was closer to the quantitative value of the shape strain. To conduct a more quantitative study in the future, we will choose an appropriate orientation from the initial austenite for observation considering the variant formation of martensite.

5. Conclusions

The submicron marker method can capture the plastic strain distribution inside lenticular martensite using electron beam lithography. The plastic strain inside the martensitic plate was larger in the middle area where the midrib had developed than in the vicinity of the interface with austenite. This outcome corresponds to the shape strain distribution estimated by PTMC based on the characteristics of the dislocations observed at the martensite/austenite interface.

Acknowledgement

This work was supported by JSPS KAKENHI Grant Number JP23K04449.

REFERENCES

1) F. Habrovec, J. Skarek and P. Rys: *Mater. Sci. Eng.*, **21** (1975), 93. https://doi.org/10.1016/0025-5416(75)90203-7
2) J. W. Morris, Jr.: *ISIJ Int.*, **51** (2011), 1569. https://doi.org/10.2355/isijinternational.51.1569
3) H. Fujii, R. Ueji and Y. Morisada: *Scripta Mater.*, **70** (2014), 39. https://doi.org/10.1016/j.scriptamat.2013.09.012
4) T. Tsuchiyama, T. Inoue and J. Tabata: *Scripta Mater.*, **122** (2016), 36. https://doi.org/10.1016/j.scriptamat.2016.05.019
5) M. S. Wechsler, D. S. Lieberman and T. A. Reed: *Trans AIME*, **197** (1953), 1503.
6) J. S. Bowles and J. K. Mackenzie: *Acta Metall.*, **2** (1954), 129. https://doi.org/10.1016/0001-6160(54)90102-9
7) N. D. H. Ross and A. G. Crocker: *Acta Metall.*, **18** (1970), 405. https://doi.org/10.1016/0001-6160(70)90126-4
8) D. P. Dunne and C. M. Wayman: *Acta Metall.*, **19** (1971), 425. https://doi.org/10.1016/0001-6160(71)90166-0
9) P. M. Kelly: *Mater. Trans. JIM*, **3** (1992), 235. https://doi.org/10.2320/matertrans1989.33.235
10) R. L. Patterson and C. M. Wayman: *Acta Metall.*, **14** (1966), 347. https://doi.org/10.1016/0001-6160(66)90094-0
11) A. Shibata, S. Morito, T. Furuhara and T. Maki: *Scripta Mater.*, **53** (2005), 597. https://doi.org/10.1016/j.scriptamat.2005.04.023
12) M. Yamamoto, K. Nishikawa, Y. Noda, I. Saburi, M. Hayakawa, M. Oka and T. Kurumizawa: *Vac. Sci. Technol.*, **B12** (l994), 1813. https://doi.org/10.1116/1.587606
13) N. Bergeon, S. Kajiwara and T. Kikuchi: *Acta Mater.*, **48** (2000), 4053. https://doi.org/10.1016/S1359-6454(00)00187-7
14) C. Efstathiou and H. Sehitoglu: *Scri. Mater.*, **59** (2008), 1263. https://doi.org/10.1016/j.scriptamat.2008.08.030
15) H. A. Padilla, J. Lambros, A. J. Beaudoin and I. M. Robertson: *Int. J. Sol. Str.*, **49** (2012), 18. https://doi.org/10.1016/j.ijsolstr.2011.09.001
16) F. Yusof, P. Lopez-Crespo and P. J. Withers: *Int. J. Fat.*, **56** (2013), 17. https://doi.org/10.1016/j.ijfatigue.2013.07.002
17) M. C. Casperson, J. D. Carroll, J. Lambros, H. Sehitoglu and R. H. Dodds, Jr.: *Int. J. Fat.*, **61** (2014), 10. https://doi.org/10.1016/j.ijfatigue.2013.11.020
18) J. C. Stinville, P. G. Callahan, M. A. Charpagne, M. P. Echlin, V. Valle and T. M. Pollock: *Acta Mater.*, **186** (2020), 172. https://doi.org/10.1016/j.actamat.2019.12.009
19) K. Hasegawa, K. Kawamura, T. Urabe and Y. Hosoya: *ISIJ Int.*, **44** (2004), 603. https://doi.org/10.2355/isijinternational.44.603
20) N. Ishikawa, K. Yasuda, H. Sueyoshi, S. Endo, H. Ikeda, T. Morikawa and K. Higashida: *Acta Mater.*, **97** (2015), 257. https://doi.org/10.1016/j.actamat.2015.06.037
21) R. F. W. Pease: *Contemp. Phys.*, **22** (1981), 265. https://doi.org/10.1080/00107518108231531
22) A. Shibata, H. Yonezawa, K. Yabuuchi, S. Morito, T. Furuhara and T. Maki: *Mater. Sc. Eng. A*, **438–440** (2006), 241. https://doi.org/10.1016/j.msea.2005.12.044
23) A. Shibata, T. Furuhara and T. Maki: *Acta Mater.*, **58** (2010), 3477. https://doi.org/10.1016/j.actamat.2010.02.022
24) A. Shibata, T. Murakami, S. Morito, T. Furuhara and T. Maki: *Mater Trans.*, **49** (2008), 1242. https://doi.org/10.2320/matertrans.MRA2007296https://doi.org/10.2320/matertrans.MRA2007296